14th International Conference on Structural Safety and Reliability - ICOSSAR'25
1-6 June, 2025 - Los Angeles California, USA
R. Ghanem, E. Johnson, S. Masri and A. Olivier (Eds)

SEISMIC ENERGY DISSIPATION AND SYSTEM FRAGILITY ANALYSIS OF CONTINUOUS REINFORCED CONCRETE HIGHWAY BRIDGES

MUHAMMAD RASHID[1] AND MAYUKO NISHIO[2]

[1]Department of Engineering Mechanics and Energy, University of Tsukuba
1-1-1 Tennodai, Tsukuba, Ibaraki, 305-8577, Japan
s2236012@u.tsukuba.ac.jp

[2]Institute of Systems and Information Engineering, University of Tsukuba
1-1-1 Tennodai, Tsukuba, Ibaraki, 305-8577, Japan
nishio@kz.tsukuba.ac.jp

Key words: Seismic Energy, Hysteretic, Damping, PSDM, Fragility, Highway Bridges.

Abstract. *The seismic resilience of bridge infrastructure is critical to ensuring the continued functionality of transportation networks during earthquakes. Traditional force- and displacement-based design approaches assess structural performance based on peak response measures. In contrast, energy-based seismic assessment offers a unified approach that inherently captures both force and deformation demands. This study examines component-level seismic energy dissipation and its impact on the global system fragility of multi-span reinforced concrete (RC) bridges. A high-fidelity finite element model was developed, and extensive nonlinear time-history analyses were conducted using a suite of real ground motion records. The distribution of hysteretic and damping energy across critical components, including columns, bearings, abutments, and shear keys, was quantified. The results indicate that hysteretic energy dissipation in bearings predominantly governs the seismic response, while damping energy remains relatively stable, governed by the structural mass and bearing properties. Component and system fragility curves reveal that components exhibiting higher energy dissipation drive system fragility. These findings advance the understanding of energy dissipation mechanisms and aid into retrofit prioritization strategies to enhance bridge resilience.*

1 INTRODUCTION

Multi-span reinforced concrete highway bridges are essential elements of transportation systems, critical for sustaining regional socio-economic activities and supporting emergency responses. Nonetheless, their susceptibility to seismic events remains a significant concern, primarily due to the intricate dynamic interplay among structural components and the uncertainties inherent in earthquake ground motions. Landmark earthquakes, including the 1994 Northridge event in the USA, the 1995 Kobe earthquake, the 2011 Tohoku event in Japan, and the 2023 Turkey-Syria earthquake, have repeatedly highlighted the vulnerability of bridge infrastructure, thereby emphasizing the pressing need for improved seismic risk assessments and resilient design strategies [1].

Effective mitigation of earthquake-induced damage necessitates a thorough understanding of seismic hazards and their interactions with structural system. Conventional design methods, which rely on force- and displacement-based evaluations of peak responses, often overlook the cumulative, energy-dependent characteristics of seismic demands. In contrast, energy-based seismic design captures force, deformation, and energy input concurrently, offering a more comprehensive and realistic depiction of structural behavior under seismic loading conditions [2].

A critical aspect of this approach is the examination of how seismic energy is distributed and dissipated within key bridge components, such as piers, bearings, shear keys, and deck connections. The pathways of energy dissipation elucidate the mechanisms by which damage initiates and progresses throughout the structure. By considering kinetic, damping, and hysteretic energies, the latter resulting from inelastic deformations, can provide valuable insights into the contributions of individual components to overall energy dissipation during an earthquake [3]. Moreover, energy-based demand parameters enable differentiation between components that may exhibit similar displacements yet endure markedly different internal force levels, thereby supporting a more precise evaluation of serviceability and damage potential.

Unlike traditional peak-deformation based engineering demand parameters (EDPs) that might neglect the cumulative aspects of ground motion, energy-based EDPs encapsulate the entire history of seismic demand. Although several studies have adopted cumulative EDPs to refine fragility modeling [4,5], establishing consistent damage state thresholds remains challenging. While displacement-based EDPs often facilitate clearer threshold definitions, they may fail to capture critical energy-related damage phenomena. Research by Quinde et al. [6] and Gentile et al. [3] has explored the relationships between deformation- and energy-based measures in frame systems, suggesting that models linked to seismic intensity measures can yield state-dependent fragility estimates. However, these studies are primarily confined to single-degree-of-freedom or frame systems and do not fully represent the distributed demands observed in multi-component bridge structures.

In this context, fragility analysis emerges as a critical probabilistic framework for quantifying the likelihood of structural systems exceeding defined damage states under varying levels of seismic intensity. However, traditional fragility methodologies often overlook the role of seismic energy demand and dissipation, thereby limiting the robustness and accuracy of vulnerability assessments. To overcome these shortcomings, the present study examines the distribution and dissipation of seismic energy in multi-span reinforced concrete highway bridges, aiming to extend classical fragility models through the explicit integration of energy-based demand parameters. The findings advance the understanding of energy-driven damage mechanisms and contribute to the refinement of seismic fragility models for critical transportation infrastructure.

2 SEIMIC ENERGY DISTRIBUTION IN STRUCTURE

The balance between earthquake input energy and the energy absorbed by a structure provides a fundamental basis for evaluating structural behavior up to failure. Earthquake input energy (*IE*), which characterizes the intensity of ground shaking, is partitioned within the structure into kinetic energy (*KE*), damping energy (*DE*), strain energy (*SE*), and hysteretic energy (*HE*). This energy balance can be expressed as:

$$IE = KE + DE + SE + HE \tag{1}$$

While various methods are available to compute these energy components, this study adopts the direct integration method. For a multi-degree-of-freedom (MDOF) system, with mass matrix $\mathbf{m}$ and velocity vector $\dot{\mathbf{u}}$, the kinetic energy which represent the work done by inertial forces is given by Eq. (2).

$$KE = \frac{1}{2}\dot{\mathbf{u}}^{\mathbf{T}}[\mathbf{m}]\dot{\mathbf{u}} \tag{2}$$

Energy dissipation through structural damping is computed as the work done by damping forces. Given the damping matrix $\mathbf{c}$, the corresponding damping energy is formulated by Eq. (3).

$$DE = \int_0^u \mathbf{d}\dot{\mathbf{u}}^{\mathbf{T}}[\mathbf{c}]\dot{\mathbf{u}} = \int_0^t \dot{\mathbf{u}}^{\mathbf{T}}[\mathbf{c}]\dot{\mathbf{u}}dt \tag{3}$$

The absorbed energy within the system consists of elastic strain energy and hysteretic energy. Strain energy arises from elastic deformation and is governed by stiffness, strength, and displacement, while hysteretic energy reflects energy dissipation through inelastic cyclic deformations. Strain energy can be evaluated using the tangent stiffness matrix $\mathbf{k_t}$ and displacement vector $\mathbf{u}$ as in Eq. (4).

$$SE = \frac{1}{2}\mathbf{u}^T[\mathbf{k_t}]\mathbf{u} \tag{4}$$

Hysteretic energy is determined as the difference between the total absorbed energy and strain energy under external force $\mathbf{F}$, given by Eq. (5).

$$HE = \int_0^u \mathbf{F}^{\mathbf{T}}\mathbf{du} - \frac{1}{2}\mathbf{u}^T[\mathbf{k_t}]\mathbf{u} \tag{5}$$

Seismic input energy is governed by structural mass and ground motion acceleration. When mass is concentrated at the nodes and element mass is neglected, *IE* can be calculated based on the interaction between ground acceleration and nodal mass, assuming a uniform excitation. However, this approach ignores phase delays, which can significantly affect the accuracy of results in large structures. For the ground motion acceleration $\ddot{\mathbf{u}}_\mathbf{g}$,the *IE* is given as follows.

$$IE = -\int_0^u \mathbf{du}^{\mathbf{T}}[\mathbf{m}]\ddot{\mathbf{u}}_\mathbf{g} = -\int_0^t \dot{\mathbf{u}}^{\mathbf{T}}[\mathbf{m}]\ddot{\mathbf{u}}_\mathbf{g}dt \tag{6}$$

3 FRAGILITY FUNCTIONS

Fragility functions are based on reliability theory to quantify the probability that seismic demand (*D*) exceeds structural capacity (*C*) for a given ground motion intensity measure (*IM*) [7,8]. This relationship is described as follows:

$$Fragility = P[D \geq C \mid IM] \tag{7}$$

Seismic demand is typically estimated through a probabilistic seismic demand model (PSDM) and structural capacities are defined based on limit states. The PSDM is expressed in

the form of power-law as in Eq. (8).

$$S_d = a\left(IM\right)^b \tag{8}$$

where S_d is the median demand and a, and b are regression coefficients of the demand data derived from nonlinear time-history analyses. Assuming a lognormal distribution for structural capacity, the fragility function for a component can be expressed as a cumulative density function described by Eq. (9).

$$P\left[D \geq C \mid IM\right] = \Phi\left(\frac{\ln\left(S_d\right) - \ln\left(S_c\right)}{\beta_{d|IM}}\right) \tag{9}$$

where Sc represent the median capacity, and $\beta_{d|IM}$ represents the dispersion of the demand conditional on the intensity measure.

While component fragility is useful in identifying the most vulnerable components and retrofit decision-making, system fragility is more significant for transportation network risk assessments [9]. Using the first order reliability theory, the bridge system can be regarded as a series or parallel system, depending on the correlation index. If all the components are considered completely correlated, the system failure will be governed by the most fragile component. On the other hand, if no correlation among component responses is considered, the system will be treated as parallel and the failure under specific limit state will reach once all the components get into that particular limit state. However, in this study, the system fragility is based on the exact correlation between component response and computed by integrating the joint probabilistic seismic demand model (JPSDM) over all possible failure domains [7]. Using Monte Carlo simulation, N random samples are generated from the resultant joint probability distribution, and the system fragility is evaluated at each IM value using the relation in Eq. (10), for which the failure samples are tracked using the indicator function IF in Eq. (11).

$$P\left[F_{sys} \mid IM\right] = \frac{\sum_{i=1}^{N} IF_i}{N} \tag{10}$$

$$I_F = \begin{cases} 1 & \text{if } \left(x_1, x_2 \ldots x_3\right) \in F_{1,2,\ldots,n} \\ 0 & \text{if } \left(x_1, x_2 \ldots x_3\right) \notin F_{1,2,\ldots,n} \end{cases} \tag{11}$$

where (x_1, x_2, x_3, …x_n) represents the random demand sample and $F_{1,\,2,\,3\ldots n}$ is the failure space defined by n components capacity limit states.

4 DESCRIPTION AND NUMERICAL MODELING OF THE BRIDGE

The bridge investigated in this study is representative of the multi-span continuous RC I-girder class, adopted from DesRoches et al. [10]. The typical span length ranges from 9 to 46 meters, utilizing standard I-shaped girders in the superstructure. Detailed descriptions of the bridge configuration and the analytical modeling approach are provided in the subsequent sections.

4.1 Structural description

A typical seat-type abutment bridge is considered in this study, reflecting common configurations found within the California bridge inventory. As most I-girder bridges feature two- or three-span layouts, a three-span configuration is selected, recognizing that two-span bridges have been extensively investigated in prior studies [11]. The bridge design represents median values from the 1971–1990 design era. The central span measures 18.29 meters, approximately 1.4 times longer than each side span. The bent columns are 6.7 meters in height, 0.91 meters in diameter, and are spaced 6.6 meters apart. Each column is reinforced with 36 #8 longitudinal bars and confined with #4 spiral ties at an 89 mm pitch. The superstructure consists of seven I-girders, each 0.91 meters deep with a flange width of 0.48 meters, spaced at 1.68-meter intervals. A 25.4 mm gap separates the deck from the abutment backfill, while shear keys are incorporated to limit lateral displacements. Soil-structure interaction is modeled through translational and rotational springs at the foundations with stiffness values of 140.1 x 10^3 kN/m and 3387 x 10^3 kN.m/rad respectively

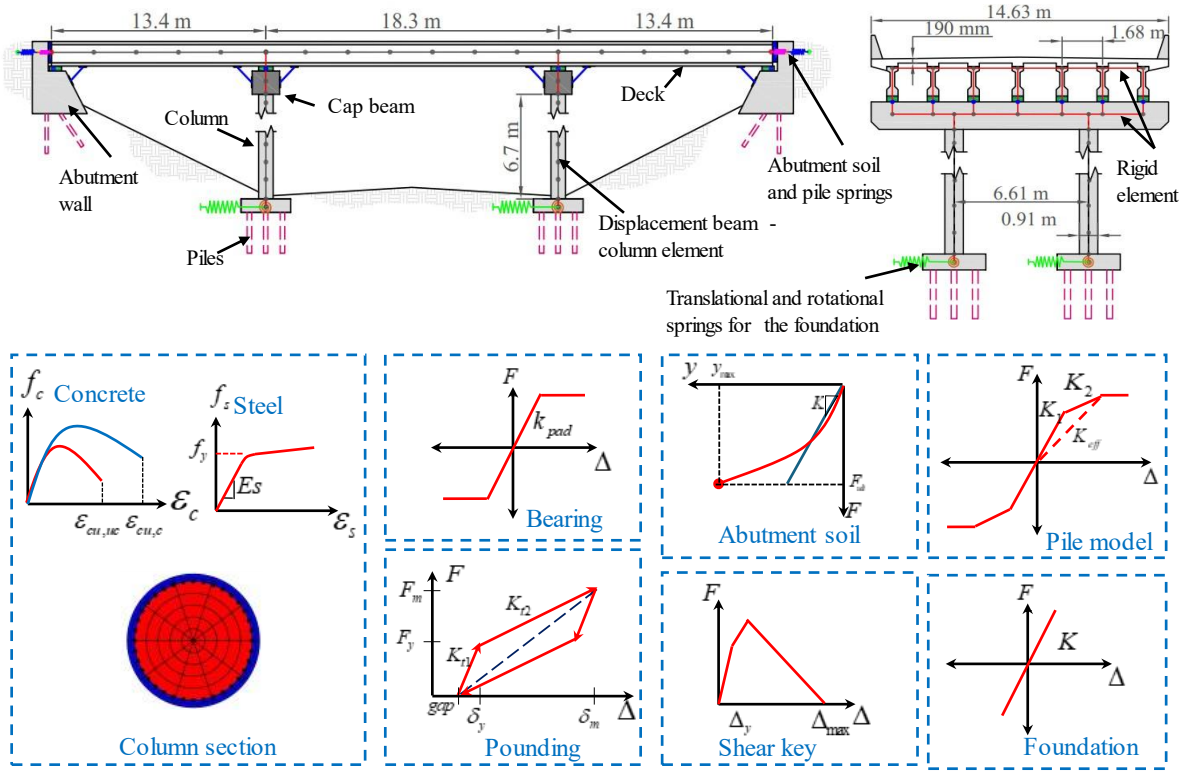

Figure 1: Layout and finite element modeling of the I-girder bridge model

4.2 Numerical modeling

The numerical modeling of the study bridge was carried out using *OpenSees*, incorporating both material and geometric nonlinearities [12]. The material properties employed in the analysis are summarized in Table 1. The bridge deck was idealized using *ElasticBeamColumn* elements, with mass lumped at discrete nodes along its length. Composite section properties,

derived from the girder geometry, were assigned accordingly. A schematic representation of the analytical modelling is provided in Fig. 1.

Nonlinear concrete behavior was simulated using the *Concrete07* material model, which is based on the Chang and Mander formulation, while the *Steel02* model was adopted for reinforcing steel to capture isotropic hardening and the Bauschinger effect. Columns were modeled as displacement-based beam-column elements with fiber sections, incorporating *P-Δ* effects. Longitudinal interaction between the bridge deck and abutment, resulting in concentrated pressures in the backfill soil, was modeled using *ZeroLengthElement* with hyperbolic gap characteristics. Passive resistance from the pile-backfill system was represented by a tri-linear soil model following the methodology proposed by Choi [13]. Deck-abutment pounding, a common phenomenon in seat-type abutment bridges, was captured using *ZeroLengthElement* with *ElasticPPGap* material properties oriented normal to the deck face to simulate contact and separation behavior [14]. Isolation bearings were modeled as bilinear elastoplastic *ZeroLengthElements*, assuming a shear modulus of 1.38 MPa and a friction coefficient of 0.4 between the concrete and bearing pads. Shear keys were represented by *ZeroLengthElement* assigned with hysteretic material properties.

Table 1: Material properties of the structural components

Bridge component	Material properties
Bearings[1]	F_y = 58.5 kN, K = 4.48 kN/mm
Columns	Unconfined concrete: f'_c = 33.8 MPa, ε_c = 0.002, f_t = 3.62 MPa, ε_t = 0.0002
	Confined concrete: f'_c = 42.9 MPa, ε_c = 0.005, f_t = 3.62 MPa, ε_t = 0.0002
	Steel: Fy = 460 MPa, Es = 2 x105 MPa, α = 0.01
Piles[1]	F_y = 124.4 kN, F_u = 177.7 kN, δ_y = 7.6 mm, δ_u = 25.4 mm
Backfill soil[2]	Fu = 444 kN, K = 20.5 kN/mm/m
Shear keys[1]	F_y = 142.2 kN, F_u = 203.1 kN, δ_y = 7.62 mm, δ_u = 25.4 mm
Pounding[1]	K_1 = 2328.7 kN/mm, K_2 = 592.39 kN/mm, Δ_{gap} = 25.4 mm, δ_y = 29.2 mm

[1] The values are associated with a single component.
[2] The mentioned values are per unit width of abutment.

5 GROUND MOTION SUITE

To evaluate the energy characteristics of various bridge components, a dataset of 269 accelerograms was compiled from the K-NET and KiK-net strong ground motion databases. These records encompass 35 seismic events recorded between 1996 and 2023 as shown in Fig. 2 (a). The acceleration response spectra of the selected ground motions, along with their median and standard deviation, are illustrated in Fig. 2(b). Selection criteria for the records included: (1) a mean peak ground acceleration (PGA) of the east-west and north-south components exceeding 0.06g, (2) a moment magnitude (Mw) greater than or equal to 5.5, (3) a focal depth less than or equal to 70 km, and (4) an average shear wave velocity (Vs30) ranging between 120 and 1400 m/s. A significant portion of the records originate from the 2011 Tohoku earthquake, contributing to the high spectral accelerations observed in the dataset.

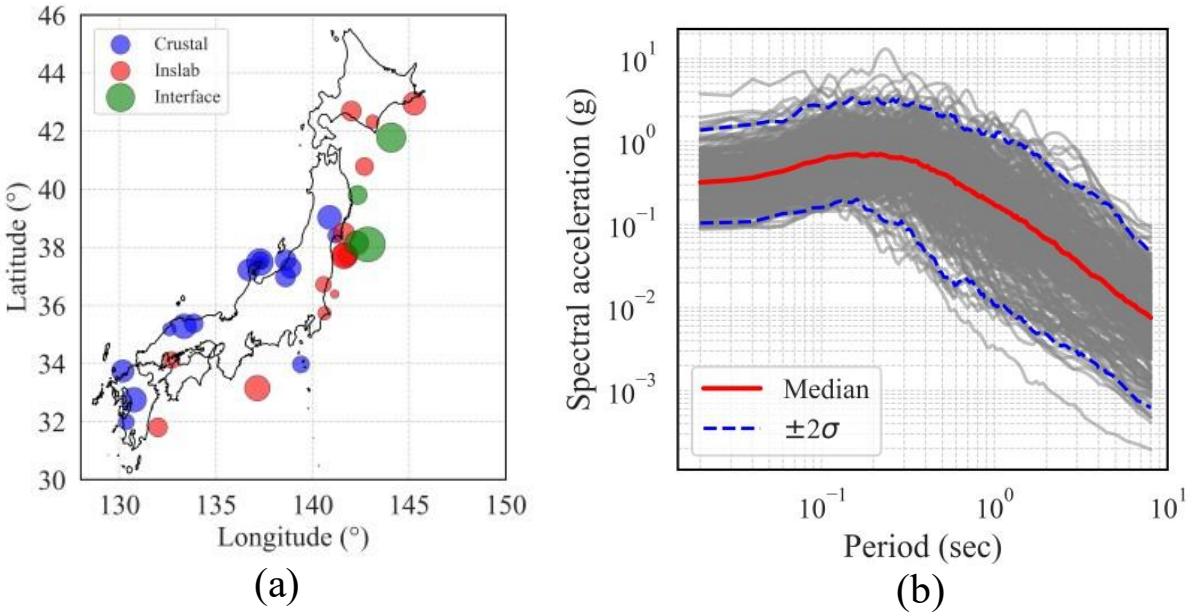

Figure 2: Selected seismic records (a) Spatial distribution and (b) Accelerations response spectra

6 RESULTS AND DISCUSSION

6.1 Seismic energy distribution for bridge components

This section describe the distribution of seismic energy among bridge components and their contributions to the overall structural energy dissipation. An initial gravity load analysis was applied, followed by dynamic time-history simulations, during which energy quantities were computed at each analysis step. To illustrate the energy distribution, a deterministic case is presented using the Type II-II design ground motion (Fig. 3a) recorded at the JR Takatori station during the 1995 Kobe earthquake.

Seismic energy components were calculated based on the formulations outlined in Section 2. Damping associated with bearings, columns, deck, piles, and soil was modeled as elemental damping, while mass-proportional damping is a function of the structural mass which is concentrated at discrete nodes in this study. At the end of seismic excitation, both damping and hysteretic energy values plateaued, whereas kinetic energy diminished to zero. Figure 3 (b) depicts the distribution of damping energy among the components and structural mass, with nodal mass damping being the most significant (~2750 kN·m), followed by abutment soil (~540 kN·m) and bearings (~260 kN·m). In contrast, the deck and bent cap-beam contributed minimally, with approximately 25 kN·m and 3 kN·m, respectively. The distribution of hysteretic energy, shown in Fig. 3c, reveals that bearings dissipated the majority of energy (~7698 kN·m), reflecting their critical role in mitigating superstructure inertial forces. Contrary, cap beams and columns exhibited lower hysteretic energy dissipation due to their higher stiffness characteristics.

The temporal evolution of energy accumulation mirrors the input accelerogram, with the majority of energy dissipating within the first 20 seconds, corresponding to the strong motion phase of the ground excitation. At the system level, the summation of damping, hysteretic, and

kinetic energies at any instant of time matched the input seismic energy, as illustrated in Fig. 3d. The cumulative hysteretic energy, approximately 11000 kN·m, was nearly three times greater than the cumulative damping energy, with its growth closely aligned with periods of high ground motion amplitude. These findings underscore the dominant role of bearings in energy dissipation, effectively reducing energy transmission to the substructure and thereby enhancing structural resilience and facilitating post-earthquake serviceability.

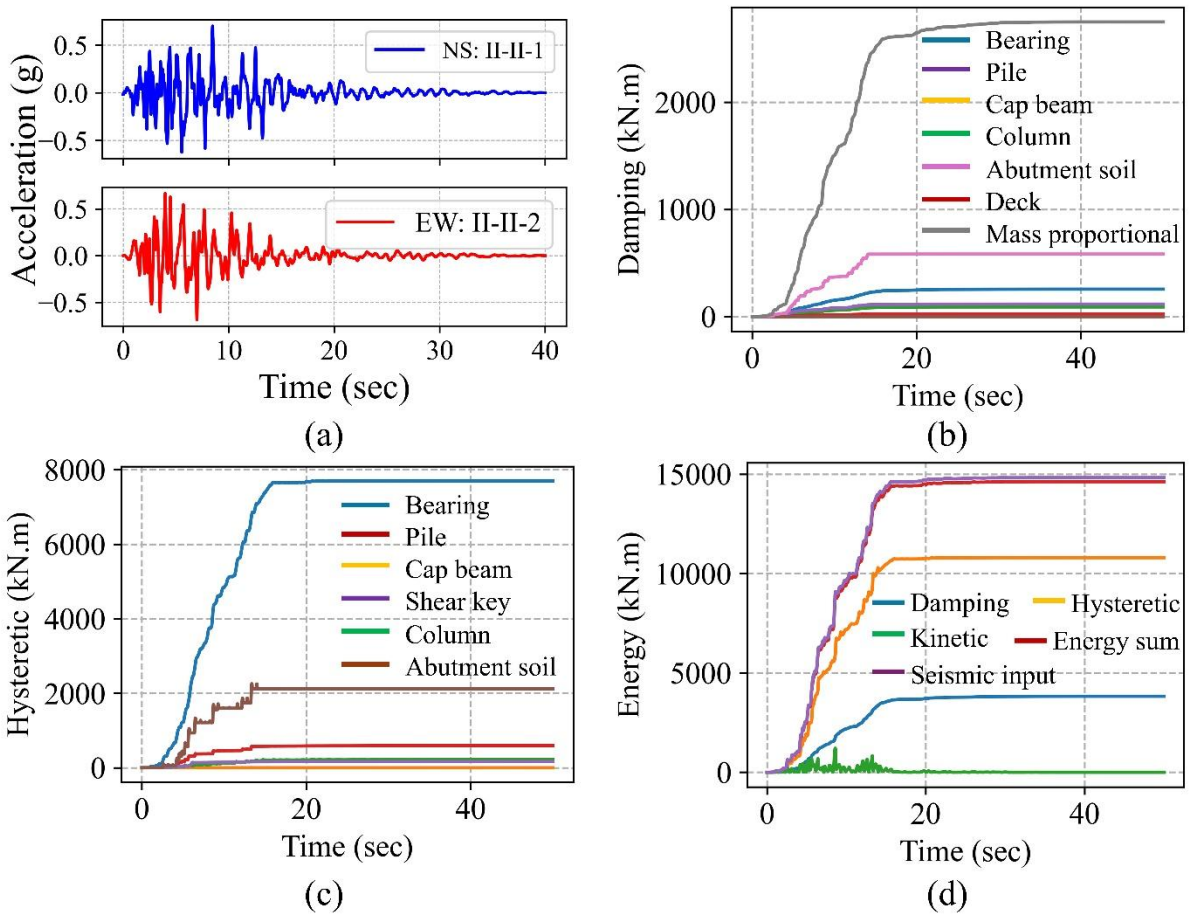

Figure 3: Seismic energy distribution for the bridge model (a) Input accelerogram for deterministic analysis (b) Damping energy (c) Hysteretic energy and (d) Bridge system energy.

6.2 Bridge components and system's fragility functions

Following extensive nonlinear time-history analyses, peak responses of critical bridge components were extracted to develop energy-based PSDMs and corresponding fragility functions using the most optimal intensity measure. Spectral acceleration at the fundamental mode (Sa_{T1}) was selected as the optimal intensity measure due to less dispersion and strong correlation with seismic demand [15]. Initially, energy-based EDPs were defined by examining the correlation between energy dissipation and peak deformation for each component, as summarized in Table 2. Following Ramanathan et al. [11], columns and deck unseating were identified as primary components due to their critical role in maintaining vertical structural

stability. Accordingly, four damage limit states, slight, moderate, extensive, and collapse, were established. Bearings and shear keys, functioning as sacrificial elements primarily contributing until moderate damage level of the bridge system, were classified as secondary components.

Table 2: Equivalent energy-based limit states for bridge components

Component EDP	Slight	Moderate	Extensive	Collapse
Column curvature ductility	1 [24.16]*	2 [79.10]	3.5 [142.09]	5 [224.74]
Deck unseating (mm)	25 [5.22]	75 [98.76]	150 [255.40]	225 [380.09]
Bearing deformation (mm)	25 [2.09]	100 [87.73]	--	--
Shear key deformation (mm)	75 [6.58]	250 [24.26]	--	--

*The values in brackets represent the equivalent dissipated energy (unit: kN·m) corresponding to the given deformation level

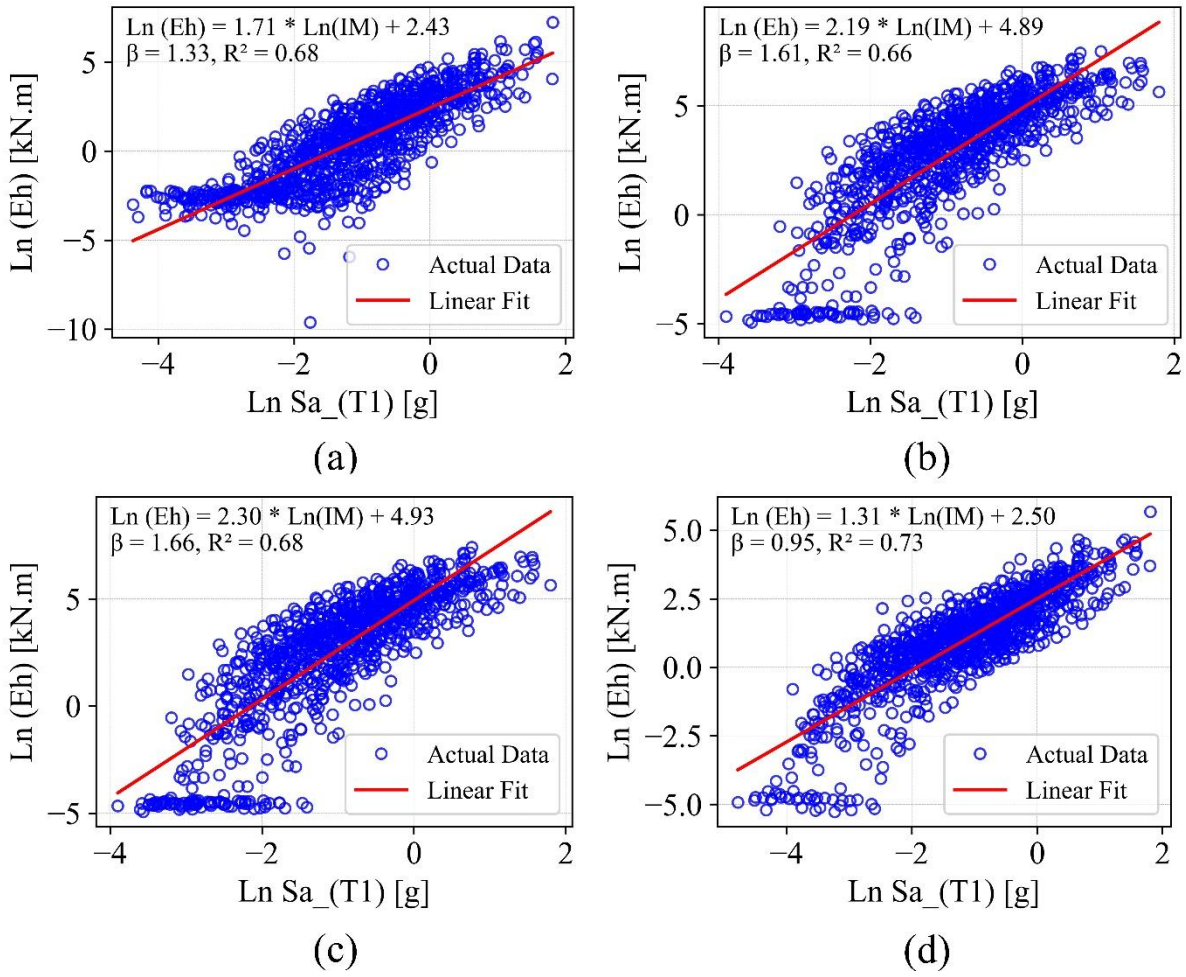

Figure 4: PSDMs for bridge components (a) Column (b) Deck unseating (c) Bearing (d) Shear key

The PSDMs for all the major components are illustrated in Fig. 4 in terms of hysteretic energy, whereas the corresponding fragility functions for all defined limit states are presented in Fig. 5. For columns, the median spectral acceleration (*Sa*) values corresponding to the slight,

moderate, extensive, and collapse states are approximately 1.36g, 2.84g, 4.17g, and 5.27g, respectively. In contrast, deck unseating exhibits lower fragility thresholds, with median *Sa* values of 0.23g for slight damage and 1.61g for moderate. As sacrificial elements, shear keys reach their median fragility at 0.62g and 1.68g for slight and moderate states, respectively. Bearings are identified as the most vulnerable components, with fragility governed by their dominant role in hysteretic energy dissipation, which also contributes to initiating deck unseating. These relative fragility patterns are consistent with the energy distribution trends shown in Fig. 3, reinforcing the capability of energy-based EDPs to capture the cumulative and progressive nature of seismic damage.

Subsequently, system-level fragility functions were derived for each limit state, along with their corresponding distribution parameters, as illustrated in Fig. 6. The overall system response appears to be strongly influenced by the performance of the bearings, owing to the adopted formulation for system fragility estimation. The median spectral acceleration values at the system level for slight, moderate, extensive, and collapse limit states are approximately 0.13g, 0.53g, 1.27g, and 1.52g, respectively.

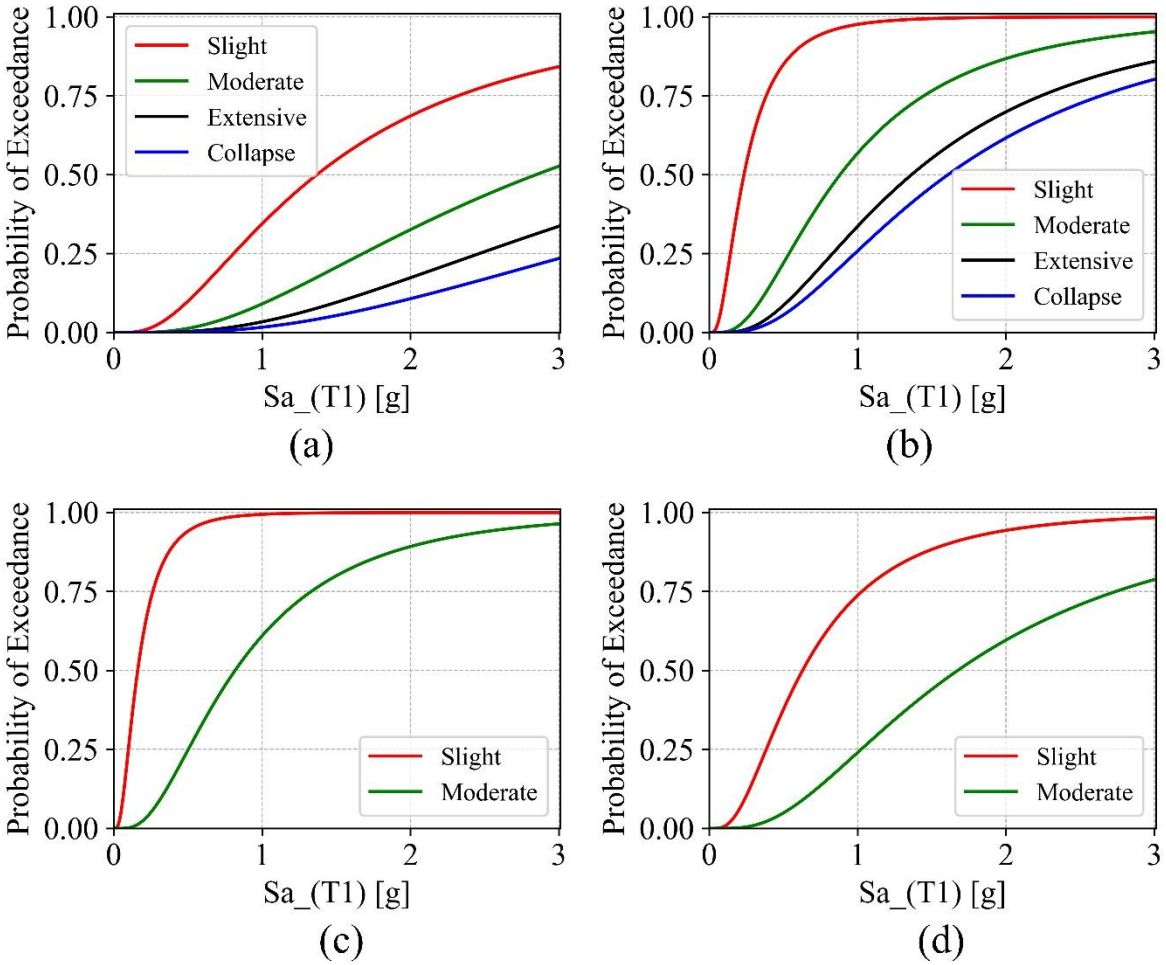

Figure 5: Fragility for bridge components (a) Column (b) Deck unseating (c) Bearing (d) Shear key

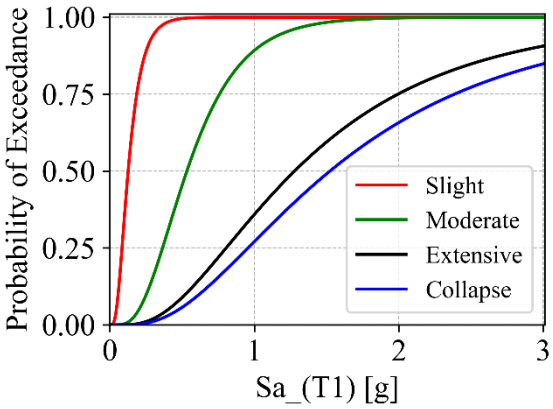

Figure 6: Energy-based fragility curves for bridge system

7 CONCLUSIONS

In this study, the energy-based seismic fragility assessment framework for reinforced concrete multi-span highway bridges, with a focus on elucidating energy distribution mechanisms and component-level contributions to global structural performance was comprehensively demonstrated. A detailed numerical model incorporating material and geometric nonlinearities was developed and subjected to extensive nonlinear time-history analyses using a suite of as-recorded real ground motions.

Energy-based EDPs were formulated by correlating cumulative energy dissipation with peak deformation for key structural components. Components were categorized as primary (columns and deck unseating) or secondary (bearings and shear keys), with distinct limit states defined for each. Fragility functions were constructed for components, which were then integrated into system fragility accounting for the exact correlation between component responses through JPSDM. Findings reveal that bearings are the most seismically vulnerable elements due to their dominant role in hysteretic energy dissipation, which also contributes to triggering deck unseating. Notably, deck unseating was observed to occur at lower seismic intensities compared to column damage, underscoring the importance of effective isolation and limiting energy transfer to the sub-structure. System-level fragility was found to be highly sensitive to bearing and deck unseating behavior, with median spectral acceleration values of 0.13g, 0.53g, 1.27g, and 1.52g corresponding to slight, moderate, extensive, and collapse damage states, respectively.

The proposed energy-based framework captures the cumulative nature of seismic demands more effectively than conventional peak-deformation based approaches and offers enhanced insight into damage progression under strong ground motion. Future research should pursue experimental validation of energy dissipation thresholds and extend this methodology to other bridge typologies to support broader applicability. The findings offer valuable implications for performance-based seismic design, retrofit prioritization, and resilience-oriented planning of critical transportation infrastructure in seismically active regions.

REFERENCES

[1] Rashid M, Nishio M. Mainshock–aftershock seismic fragility assessment of civil structures: A state-of-the-art review. *Earthquake Engineering and Resilience* 2024;3:548–73. https://doi.org/10.1002/eer2.105.

[2] Jamnani HH, Amiri JV, Rajabnejad H. Energy distribution in RC shear wall-frame structures subject to repeated earthquakes. *Soil Dynamics and Earthquake Engineering* 2018;107. https://doi.org/10.1016/j.soildyn.2018.01.010.

[3] Gentile R, Galasso C. Hysteretic energy-based state-dependent fragility for ground-motion sequences. *Earthq Eng Struct Dyn* 2021;50. https://doi.org/10.1002/eqe.3387.

[4] Kunnath SK, Chai YH. Cumulative damage-based inelastic cyclic demand spectrum. *Earthq Eng Struct Dyn* 2004;33. https://doi.org/10.1002/eqe.363.

[5] Chai YH. Incorporating low-cycle fatigue model into duration-dependent inelastic design spectra. *Earthq Eng Struct Dyn* 2005;34. https://doi.org/10.1002/eqe.422.

[6] Quinde P, Terán-Gilmore A, Reinoso E. Cumulative Structural Damage Due to Low Cycle Fatigue: An Energy-Based Approximation. *Journal of Earthquake Engineering* 2021;25. https://doi.org/10.1080/13632469.2019.1692736.

[7] Nielson BG, DesRoches R. Seismic fragility methodology for highway bridges using a component level approach. *Earthq Eng Struct Dyn* 2007;36:823–39. https://doi.org/10.1002/eqe.655.

[8] Rashid M, Nishio M. System Fragility Analysis of a Horizontally Curved Multi-span Highway Bridge Structure. *EVACES, Lecture Notes in Civil Engineering*, vol. 433 LNCE, 2023, p. 500–10. https://doi.org/10.1007/978-3-031-39117-0_51.

[9] Rashid M, Nishio M. System fragility evaluation of a curved highway bridge structure considering multi-direction seismic excitations. *Advances in Structural Engineering* 2023;26:2672–92. https://doi.org/10.1177/13694332231198136.

[10] DesRoches R, Padgett J, Ramanathan K, Dukes J. *Feasibility Studies for Improving Caltrans' Bridge Fragility Relationships* . California: 2012.

[11] Ramanathan K, Padgett JE, DesRoches R. Temporal evolution of seismic fragility curves for concrete box-girder bridges in California. *Eng Struct* 2015;97:29–46. https://doi.org/10.1016/j.engstruct.2015.03.069.

[12] McKenna F. OpenSees: A framework for earthquake engineering simulation. *Comput Sci Eng* 2011;13. https://doi.org/10.1109/MCSE.2011.66.

[13] Choi E. *Seismic analysis and retrofit of mid-America bridges*. 2002.

[14] Muthukumar S, DesRoches R. A Hertz contact model with non-linear damping for pounding simulation. *Earthq Eng Struct Dyn* 2006;35. https://doi.org/10.1002/eqe.557.

[15] Rashid M, Nishio M. An optimal intensity measure-based seismic fragility surfaces for curved bridges considering their sensitivity to seismic excitation direction. *Earthquake Engineering and Engineering Vibration* 2024.